BRNO UNIVERSITY OF TECHNOLOGY
VYSOKÉ UČENÍ TECHNICKÉ V BRNĚ

FACULTY OF MECHANICAL ENGINEERING
FAKULTA STROJNÍHO INŽENÝRSTVÍ

INSTITUTE OF PHYSICAL ENGINEERING
ÚSTAV FYZIKÁLNÍHO INŽENÝRSTVÍ

GRAPHENE DOPAMINE BIOSENSOR AND GATE EFFECT
GRAFENOVÝ BIOSENZOR DOPAMINU A VLIV HRADEL

BACHELOR'S THESIS
BAKALÁŘSKÁ PRÁCE

AUTHOR
AUTOR PRÁCE

Kateřina Krajíčková

SUPERVISOR
VEDOUCÍ PRÁCE

doc. Ing. Miroslav Bartošík, Ph.D.

BRNO 2023

Assignment Bachelor's Thesis

Institut:	Institute of Physical Engineering
Student:	**Kateřina Krajíčková**
Degree programm:	Physical Engineering and Nanotechnology
Branch:	no specialisation
Supervisor:	**doc. Ing. Miroslav Bartošík, Ph.D.**
Academic year:	2022/23

As provided for by the Act No. 111/98 Coll. on higher education institutions and the BUT Study and Examination Regulations, the director of the Institute hereby assigns the following topic of Bachelor's Thesis:

Graphene dopamine biosensor and gate effect

Brief Description:

Due to its biocompatibility and high surface electronic sensitivity, graphene is an ideal candidate for use in biosensors. A suitable design arrangement for such biosensors is in the form of a field–effect transistor (FET). In classical transistors, a lower solid–state gate is used, whereas in biological applications, an upper gate is often used, which is connected directly through the detected solution of the relevant biochemical substance. This thesis will deal with the possibilities of increasing the efficiency of the resistance response of the biosensor when using both gates, the effect of changes in the distance of the upper gate on the conductivity of the sensor channel during the detection of dopamine (and eventually selected suitable DNA fragments).

Bachelor's Thesis goals:

1. Do literature retrieval on the mentioned issue.
2. Study the transport response of the biosensor to different concentrations of dopamine solution, while observing the effect of:
a. Top gate distances and voltages.
b. Lower gate voltage.
c. Various combinations of upper and lower gate settings.
3. Suggest ways to make an existing sensors more efficient when using both gates.

Recommended bibliography:

CASTRO NETO, A. H., F. GUINEA, N. M. R. PERES, K. S. NOVOSELOV a A. K. GEIM. The electronic properties of graphene. Reviews of Modern Physics. 2009, 81(1), 109-162. ISSN 0034-6861. Dostupné z: doi:10.1103/RevModPhys.81.109.

SCHEDIN, F., A. K. GEIM, S. V. MOROZOV, E. W. HILL, P. BLAKE, M. I. KATSNELSON a K. S. NOVOSELOV. Detection of individual gas molecules adsorbed on graphene. Nature Materials. 2007, 6(9), 652-655. ISSN 1476-1122. Dostupné z: doi:10.1038/nmat1967
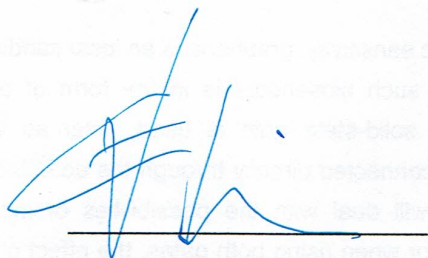
KUJAWSKA, Małgorzata, Sheetal K. BHARDWAJ, Yogendra Kumar MISHRA a Ajeet KAUSHIK. Using Graphene-Based Biosensors to Detect Dopamine for Efficient Parkinson's Disease Diagnostics. Biosensors. 2021, 11(11). ISSN 2079-6374. Dostupné z: doi:10.3390/bios11110433

BARTOŠÍK, Miroslav, Jindřich MACH, Jakub PIASTEK, David NEZVAL, Martin KONEČNÝ, Vojtěch ŠVARC, Klaus ENSSLIN a Tomáš ŠIKOLA. Mechanism and Suppression of PhysisorbedWater-Caused Hysteresis in Graphene FET Sensors. ACS Sensors. 2020, 5(9), 2940-2949. ISSN 2379-3694. Dostupné z: doi:10.1021/acssensors.0c01441.

TRIPSKÝ, Andrej. Design, fabrication and testing of graphene biosensors. Brno, 2020. Diplomová práce. Vysoké učení technické v Brně, Fakulta strojního inženýrství, Ústav fyzikálního inženýrství.
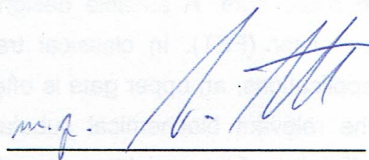
Students are required to submit the thesis within the deadlines stated in the schedule of the academic year.

In Brno, 1. 11. 2022

L. S.

prof. RNDr. Tomáš Šikola, CSc.
Director of the Institute

doc. Ing. Jiří Hlinka, Ph.D.
FME dean

Abstract

This bachelor's thesis focuses on investigating the interaction between biochemical substances (dopamine solutions) and graphene, using field-effect transistor (FET) based sensors. Graphene possesses unique properties, including biocompatibility, high charge carrier mobility, and surface sensitivity, making it an ideal material for biosensing devices. In these sensors, graphene is employed as the conductive sensing channel within field-effect transistors. By utilizing sensors with an FET arrangement, the doping of graphene induced by adsorbed atoms or molecules can be experimentally determined through the observation of the shift in the position of the Dirac point. The measurements can be performed using either the bottom-gated or electrolytic top-gated configuration of the FET sensor, and the thesis explores the differences between the two setups. Furthermore, it investigates the impact of the distance between the graphene and top-gate electrode on the sensor's response. The results of these measurements are represented by transfer curves, which exhibit characteristic peaks indicating the charge neutrality point, known as the Dirac point, of graphene.

Abstrakt

Tato bakalářská práce se zaměřuje na zkoumání interakce biochemických látek (roztoků dopaminu) s grafenem pomocí senzoru založených na polem řízeném tranzistoru (FET). Grafen má jedinečné vlastnosti, včetně biokompatibility, vysoké mobility nosičů náboje a povrchové citlivosti, což ho činí ideálním materiálem pro biosenzory. V těchto senzorech je grafen využíván v FET jako vodivý kanál citlivý na povrchové změny. Použitím senzoru s FET uspořádáním je možné experimentálně stanovit dopování grafenu způsobené adsorbovanými atomy nebo molekulami prostřednictvím pozorování posunu polohy Diracova bodu. Měření lze provádět pomocí konfigurace s dolním hradlem nebo elektrolytické konfigurace s horním hradlem FET senzoru a tato práce zkoumá rozdíly mezi těmito dvěma uspořádáními. Dále se zkoumá vliv vzdálenosti mezi grafenem a elektrodou horního hradla na odezvu senzoru. Výsledky těchto měření jsou vyjádřeny pomocí přenosových křivek, které vykazují charakteristické vrcholy indikující stav grafenu s rovnovážným stavem náboje grafenu, známé jako Diracův bod.

Keywords

graphene, biosensor, field-effect transistor, dopamine, Dirac point, Debye length, transport response

Klíčová slova

grafén, biosenzor, polem řízený tranzistor, dopamin, Diracův bod, Debyeova délka, transportní odezva

Contents

Introduction

This thesis is focused on the application of the graphene field-effect transistor (GFET) biosensor for distinguishing dopamine.

Graphene is an exceptionally thin, two-dimensional material composed of a single layer of carbon atoms arranged in a hexagonal lattice. Its unique properties make it extremely useful as a biosensor material for multiple reasons.

Graphene has high surface-to-volume ration due to its planar structure, which provides a large surface area for biomolecule immobilization, allowing for enhanced sensitivity and improved detection limits. This feature is crucial in biosensing, where interactions between target analytes and the sensing surface need to be maximized.[1]

Because of its high charge carrier mobility, graphene is an excellent conductor of electricity. This property enables the detection of biomolecular interactions through electrical signals. Changes in the conductivity of graphene-based biosensors can be correlated with the presence or concentration of a target analyte.

Graphene is biocompatible, which means it is well-tolerated by living organisms and cells. This makes it suitable for direct interaction with biological samples without causing adverse effects. Graphene-based biosensors can be used for real-time monitoring of biological processes, such as detecting biomarkers or studying cellular behavior. [2]

Furthermore GFET-based sensors exhibit rapid response times, enabling real-time monitoring. Changes in the electrolyte concentration cause measurable changes in the electrical conductivity of graphene, allowing for fast detection.[3]

Moreover GFETs can be functionalized with specific molecules or nanoparticles that selectively interact with measured solution, enhancing the sensor's selectivity and reducing interference from other substances.[4]

Finally GFET biosensors can be miniaturized to nanoscale dimensions, enabling their integration into compact and portable devices. This miniaturization allows for point-of-care applications.[5]

Dopamine is a hormone produced in the ventral tegmental area [1] [6] and can be found in the nervous system, specifically at the synapses. It is called the hormone of reward or motivation, as it is flushed out when we've successfully completed a task. Because drugs such as cocaine induce higher production of dopamine, it is said to be one of the causes behind addiction creation.[8]

Its second significance is an inhibitor, meaning that dopamine helps to control body movement. If the dopamine synapses are damaged, it may lead to Parkinson's disease, ADHD, Schizophrenia and others. [9]

The detection of dopamine and the determination of its concentration using a graphene-based sensor would, for the reasons mentioned, represent progress in medical diagnostics.

---

[1] group of neurons located close to the midline on the floor of the midbrain [7]

1. Theory

1.1. Graphene

1.1.1. Properties

Graphene is an atomically-thin material made of a two-dimensional hexagonal lattice of carbon atoms, which are spaced 1.42 Å. This structure, with each carbon atom sharing three of its four electrons in covalent bonds with its nearest neighbors (sp^2 bonds), is at the root of the robust mechanical properties of graphene.[10] At the same time, the remaining electron is delocalized over the two-dimensional lattice in a π orbital responsible for most of the material's electronic and optoelectronic properties.[11, 12] This novel material was first isolated by Geim and Novoselov in 2004 [13], they were awarded the Nobel prize in physics in 2010 for graphene discovery and study of its properties.

To better understand its properties, it is important to have a good apprehension of graphene structure. Just as its honeycomb structure, the Brillouin zone has a hexagonal structure as well. The corners are marked as K, K', which are highly symmetrical points at the energy E, where the valence and conductance bands are touching. These points are called Dirac points. In pristine graphene, the Fermi level (E_F) intersects these points.[14, 15]
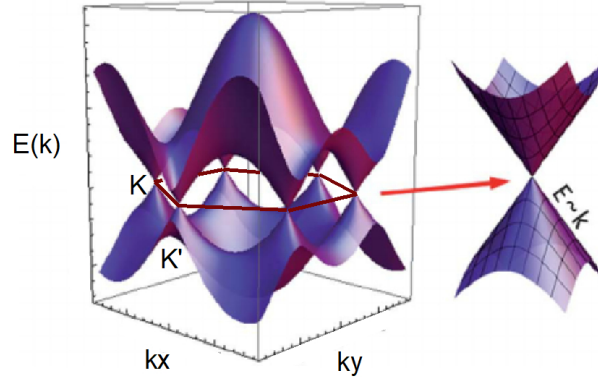
Figure 1.1: The electronic band structure of graphene with the detail of the linear part close to the Dirac point. Adapted from [16]

As the valence and conductance bands are directly connected, graphene can be described as a semiconductor with zero band gap. Moreover, the energy has a linear dependency on wave vector close to the Dirac points. Due to this one-of-the-kind characteristic, the charge carriers behave similarly as relativistic massless particles moving at the Fermi speed $v_F \approx 10^6$ m/s in Dirac points. Because of ambipolar effect, graphene can be converted from hole to electron conductance by applying an external electric field.[17]

Apart from exceptional electronic properties, graphene exhibits high resistance to in-plane deformations characterized by Young modulus $E = 1$ TPa [18] for defect-free graphene, light transmittance of 97.7 % [19] or high in-plane thermal conductivity of 5000 W/mK [20, 17].

1.1.2. Fabrication

There are many physical and chemical approaches to graphene fabrication. Some of them use the top-down technique (exfoliation, graphene oxide reduction), others take advantage of the bottom-up method (chemical vapour deposition, chemical synthesis, molecular beam epitaxy). These methods are shown in Fig. 1.2, where the quality and production costs are compared.

The two most commonly used methods (mechanical exfoliation and chemical vapour deposition) are going to be described in following chapters.
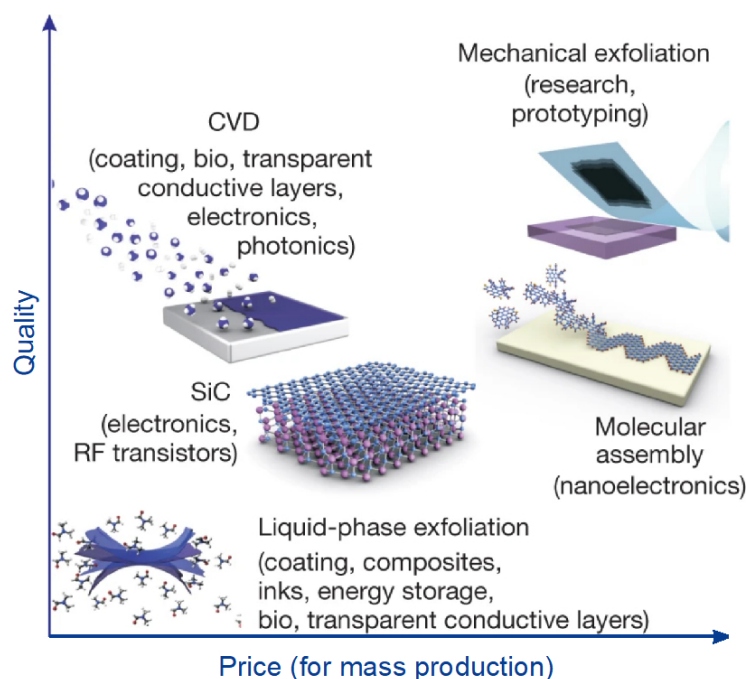
Figure 1.2: Different mass fabrication methods of graphene compared in terms of quality and price. Adapted from [21]

Exfoliation

Graphene exfoliation is a process of separating single-layer or few-layer graphene flakes from bulk graphite. The production of graphene via exfoliation is of great interest due to its simplicity and ability to prepare graphene flakes of a high quality. There have been several methods developed for exfoliating graphene, such as mechanical exfoliation, liquid-phase exfoliation, and chemical exfoliation.[22]

One of the most common methods for exfoliating graphene is mechanical exfoliation, which involves using adhesive tape to peel off thin layers of graphene from a graphite sample. This method was first demonstrated by Novoselov and Geim in 2004 [13] and has since become a widely used technique for producing high-quality graphene flakes for research purposes.[23]

Chemical vapour deposition

Chemical vapour deposition (CVD) is a promising technique for synthesizing graphene due to its ability to produce large-area, low-cost, high-quality graphene films with excellent control over the film thickness and morphology. In CVD graphene synthesis, a hydrocarbon gas, such as methane, is introduced into a reactor chamber along with a metal catalyst, typically copper, nickel or platinum, and the reaction takes place at elevated temperatures.[24]

The CVD process involves several steps, including nucleation of the graphene layer on the metal catalyst surface and growth of the graphene layer. The nucleation step is critical for producing a high-quality graphene film, and it depends on the quality and cleanliness of the metal catalyst surface, as well as the reaction conditions, such as the gas flow rate and temperature.[25]

Once the graphene film is synthesized on the metal catalyst, it needs to be transferred onto a substrate for further use. The transfer process typically involves etching away the metal catalyst, followed by transferring the graphene film onto the desired substrate using wet transfer method.[28]

Many experimental results have shown that exfoliated graphene has a much higher detection limit compared with CVD graphene due to its superior mobility.[29] However, it is not used in applications because of the inability to affect the size of the flakes and number of layers.

1.2. Graphene field-effect transistor

There are many designs of sensors, however the one that stands out for its high sensitivity, low limit of detection due to amplifying functions of transistors, fast response and rather simple test procedure is graphene field effect transistor (GFET) based sensors. A FET is a device usually used as a logical switch and consists of three electrodes – source (S), drain (D), and gate (G). Between the source and the drain there is a graphene channel (Fig. 1.3). The channel is separated from the gate electrode by an insulating layer. In biosensors, the graphene channel is also an active detection layer for sensing biomolecules.

The current I_{sd} which flows through the channel can be modulated by the gate voltage V_g. In the case of a graphene FET, the conductive channel made of graphene is capable of using both holes and electrons as charge carriers due to its ambipolar character. Gate voltage then affects not only the type and density of charge carriers with a shift of graphene Fermi level, but also a corresponding current flowing through the channel.

When the Fermi level crosses the Dirac point, graphene has the lowest charge carrier density (given mainly by temperature) and minimum electrical conductivity. The corresponding gate voltage is called the Dirac point voltage (V_{DP}) of the graphene device. Because of its semi-metal nature, graphene behaves as an electron-conductor at the positive gate voltage of V_{DP} and acts as a hole-conductor at a negative gate voltage of V_{DP}.[30]
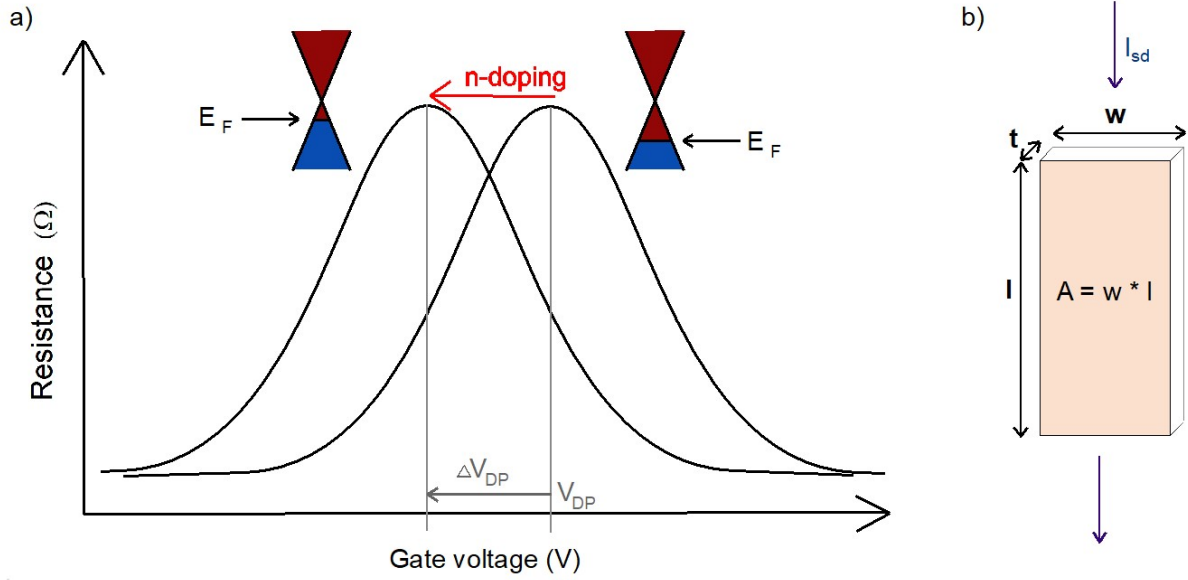
Figure 1.3: a) The shift in the Dirac point voltage and Fermi energy during n-doping; b) The graphene channel.

For GFET biosensors, conductivity is changed by the adsorption of charged ions or biomolecules. Molecules n-dope or p-dope graphene, which leads to left or right shift of the V_{DP}. For instance, the V_{DP} of the device will move to the low voltage and the conductance will go up with an increase of electrons in graphene (Fig. 1.3). A typical transfer curve for GFET shows the peak of maximal resistance at V_{DP}. Graphene FET shows to be a promising sensor due to high sensitivity to its surface changes, biocompatibility and low background noise

1.2.1. Theory behind GFET biosensors

The graphene field effect transistor consists of a silicon substrate usually used as a bottom gate, a thin layer of silicon dioxide as an insulator and two golden electrodes (source and drain) connected by a graphene channel. In case of top gate, the sample solution works as an insulator between graphene and the gate, which is usually made of a biocompatible wire that is inserted into the solution droplet. The Si substrate is used for the bottom gate and is insulated from the graphene channel by SiO_2.

The bottom and top gate function can be approximatelly described as a parallel-plate capacitor where the density of charge carriers in graphene can be determined by the gate voltage. The capacitance of a parallel-plate capacitor is

$$C = \varepsilon_0 \varepsilon_r \frac{A}{d} \tag{1.1}$$

and it can be also defined as the ratio of charge and voltage

$$C = \frac{Q}{V_g} \tag{1.2}$$

8

If the surface (aerial) concentration of majority carriers equals

$$n_A = \frac{Q}{Ae} \tag{1.3}$$

then after combining the three equations above we get

$$n_A = \frac{\varepsilon_0 \varepsilon_r}{ed} V_g \ , \tag{1.4}$$

where ε_0 is the permittivity of vacuum, ε_r the relative permittivity of the dielectric (the water solution or SiO_2), V_g is the gate voltage, e is the elementary charge and d can be either the Debye length in case of top-gate, or the distance between graphene and the bottom gate.

When applying positive voltage to the top gate, anions from the sample solution create a layer around the tip (wire). At the same time cations are immobilised on the graphene surface while the rest of the ions create a diffuse layer between the graphene and the top gate. This model is called an electric double layer, whose thickness can be approximated by the Debye length λ_D depending on the ionic strength I of the electrolyte as [17]

$$\lambda_D = \sqrt{\frac{\varepsilon_0 \varepsilon_r k_B T}{2N_A e^2 I}} \ , \tag{1.5}$$

where k_B is the Boltzmann constant, T is the temperature and N_A the Avogadro constant.

Ions at a further distance than λ_D are screened by the electric double layer which disables them from interacting with graphene. Therefore the desire is to have a larger Debye length, which makes it possible to measure at greater distances thereby increasing the device's sensitivity. A new way of increasing the λ_D could be by curving the morphology of the sensing material.[31]
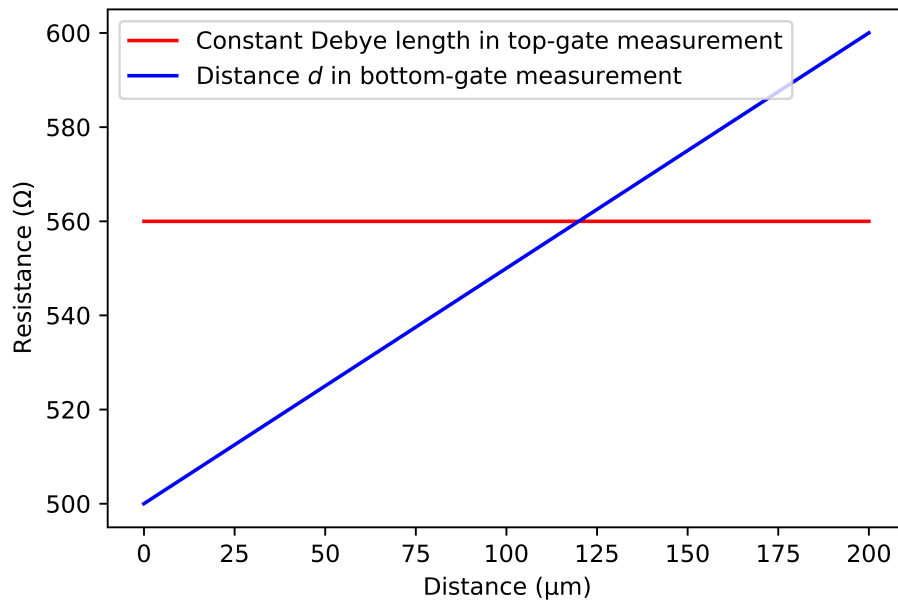

Figure 1.4: Possible dependence of resistance on distance.

Using the Ohm's law and current density derived from the Drude's model. The resistance of the graphene channel can be expressed as

$$R = \frac{V_{sd}}{n_A e v_d w} \ ,$$ (1.6)

where V_{sd} is the voltage between the source and the drain, v_d is drift velocity and w the width of the sample. Now we can express n_A as in equation (1.4) and the final result is dependency of resistance on distance as

$$R = \frac{V_{sd}}{\varepsilon_0 \varepsilon_r v_d w V_g} d$$ (1.7)

In bottom-gate measuring, the distance corresponds to the thickness of SiO_2, which represents the dielectric in the parallel-plate capacitor conception. If the d was adjustable, then the resistance would linearly rise as suggests Fig. 1.4. For top-gate measurements, the distance d is substituted with λ_D. It is assumed that the Debye length remains constant regardless the distance between the top-gate electrode and the sample. But, what if it can be altered by close proximity of the top gate?

1.2.2. Different gates of GFET biosensor

The gate first used and measured the most in experiments was the top gate. The advantage of the top-gate setup (Fig. 1.5) is that it needs only maximum of 2 V for measuring, which limits redox reactions and molecules splitting. Also as its insulator is electrolyte, there is no risk of a breach.

Because the thin layer of SiO_2 is used as an insulator for bottom-gate measurements, the distance between the gate and the channel cannot be changed, which simplifies the measuring and the processing of data. The biggest advantage is that it enables the measuring of gas phase samples. On the other hand, the bottom gate can be breached by applying too high voltage meaning it will not properly function ever again.

A dual-gate setup combines both gate electrodes; the top gate submerged into the electrolyte, as well as the bottom gate connected to Si. This setup enables measurement with higher sensitivity and to evaluate measurements depending on bottom-gate voltage, top-gate voltage and distance or concentration used.
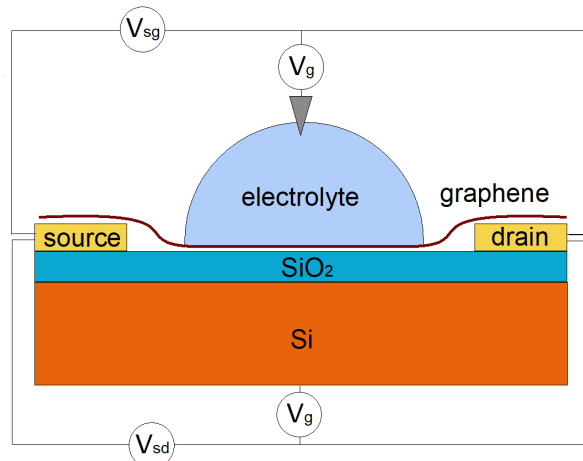

Figure 1.5: Top and bottom-gate measurement setup.

1.3. Dopamine

Dopamine is a neurotransmitter that plays a crucial role in a wide range of physiological and psychological processes in the human body.[32] It is a monoamine and belongs to the catecholamine family of neurotransmitters. Dopamine is synthesized from the amino acid tyrosine in specialized cells called dopaminergic neurons, which are located in various regions of the brain and peripheral nervous system.[33]

Dopamine functions as a neurotransmitter in the synapses of the brain, playing a crucial role in various physiological processes. Upon release, dopamine binds to specific receptors on the postsynaptic membrane, initiating a cascade of intracellular events. These signaling pathways contribute to the regulation of motor control, reward and motivation, and cognitive processes such as attention and memory.[34] It is also involved in regulating the release of other neurotransmitters such as serotonin and norepinephrine. Dysregulation of dopamine signaling has been implicated in a variety of neurological and psychiatric disorders, including Parkinson's disease, schizophrenia, and addiction.[35]

The dopamine system consists of several pathways in the brain, including the mesolimbic and mesocortical pathways, which play a key role in reward and motivation.[36] The mesolimbic pathway is involved in the processing of reward, pleasure, and motivation, and is implicated in addiction and substance abuse. The mesocortical pathway projects to the prefrontal cortex and is involved in cognitive processes such as attention, working memory, and decision-making.[37]
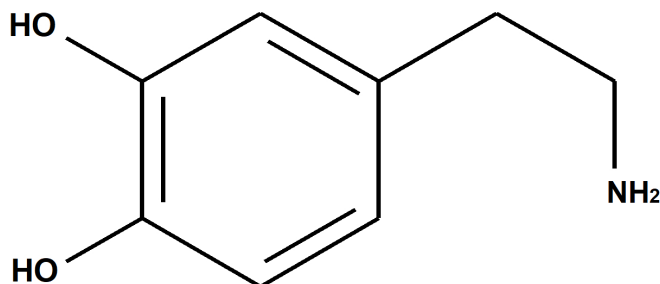
Figure 1.6: The structure of dopamine.

Dopamine signalling is regulated by a complex interplay of factors, including the activity of dopaminergic neurons, the availability of dopamine precursors such as tyrosine, and the activity of enzymes that synthesize and degrade dopamine. For example, the enzyme tyrosine hydroxylase is the rate-limiting step in dopamine synthesis and is regulated by feedback inhibition and other mechanisms.[38]

Abnormal dopamine signaling has been implicated in a variety of neurological and psychiatric disorders.[39] For example, Parkinson's disease is a neurodegenerative disorder characterized by the loss of dopaminergic neurons in the substantia nigra, leading to a deficiency of dopamine in the basal ganglia and resulting in motor symptoms such as tremors and rigidity.[40] Treatment for Parkinson's disease often involves administering

dopamine agonists, which stimulate dopamine receptors, or levodopa, which is converted to dopamine in the brain.[41]

Schizophrenia is a psychiatric disorder characterized by delusions, hallucinations, and disorganized thinking.[42] Abnormal dopamine signaling has been implicated in the pathophysiology of schizophrenia, specifically in the mesolimbic pathway. Antipsychotic medications, such as dopamine antagonists, are commonly used to treat schizophrenia and block dopamine signaling in the brain.[43]

Addiction is a complex disorder characterized by compulsive drug seeking and use, despite negative consequences. The mesolimbic dopamine pathway plays a key role in addiction, as drugs of abuse can activate this pathway and lead to increased dopamine release in the nucleus accumbens, a brain region associated with reward and motivation. Chronic drug use can lead to changes in the dopamine system, such as decreased dopamine receptor availability and decreased dopamine release, which can contribute to addiction and withdrawal symptoms.[39]

2. Experiments and results

2.1. Experimental setup

The sample (graphene on SiO_2 on Si substrate) is glued with silver conductive paste on a conductive sample carrier with female pins welded at the edge of the carrier. By ultrasonic bolder, conductive paths from gold are created between lithographic contacts and the pins.

The current source connected serially to a 1 MΩ resistor creates gate voltage between the gate (either top or bottom) and the ground. To measure resistance, a lock-in amplifier is connected to the circuit between the source and the drain. Before reaching the source electrode signal passes through a 10 MΩ resistor. The expected order of measured solution resistance is a maximum of 10^3 kΩ therefore all the current flows through the graphene layer and none leaks.

To adjust all parameters of the experiment and to save measured data, an interface designed in LabView is used. [44]
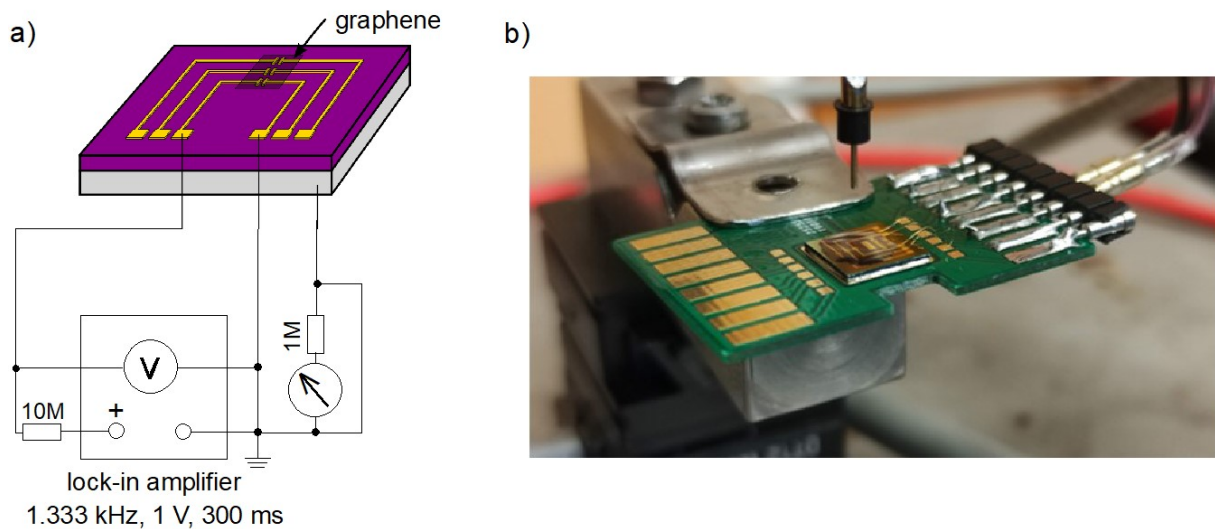
Figure 2.1: a) Schematic circuitry of the experimental setup [45]; b) Photo of the sample with smaller water droplet on a holder with top-gate tip, connected with pins.

2.2. Top-gate GFET biosensor

2.2.1. Measurement procedure

At the beginning of each measurement, it is necessary to place the sample on a holder and plug it in according to Fig. 2.1 a). The holder can be positioned in x and y directions, whereas a micrometer screw moves the tip used as a top-gate in z direction.

After the sample is attached to a holder and plugged into the circuit, zero distance has to be found. The tip is slowly lowered by the micrometer screw and the goal is to approach the tip and its reflection on the sample to reach the shortest possible distance

and not to damage the samples' surface. The z position is marked down for later use, then the tip is raised and a solution droplet of volume 50 µl is pipetted onto the sample.

Then the electrical setup is arranged. Compliance (a limitation to prevent the gate from being breached) is set to 2 V. If a more simple experiment is performed, the gate voltage is set at desired constant and measuring can begin. For a more complex measurement it is essential to create a saw voltage, beginning at 0 V, increasing up to 1.5 V, decreasing down to -1.5 V and ending back at 0 V. The individual voltage step is ± 0.01 V per 0.5 s.
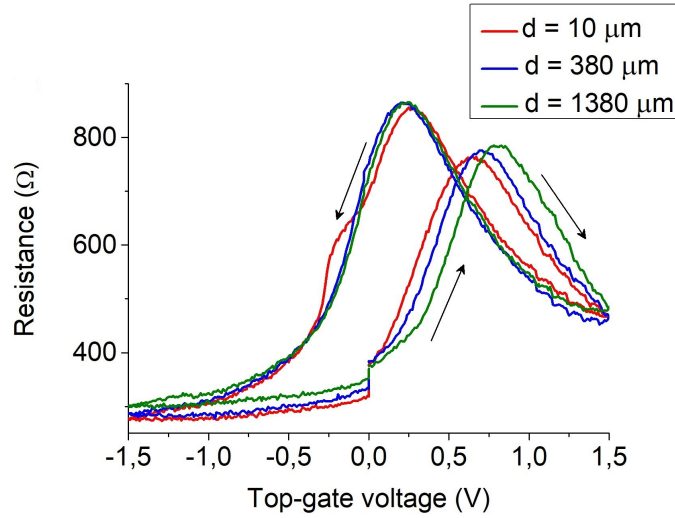

Figure 2.2: Top-gate transport response of Dopamine 10 mM at three different distances.

A set of measurement for one concentration was mostly done by using the saw voltage described in the previous paragraph while changing the distance between the end of the tip and the sample surface (changing z-position) after each round of voltage change was completed. Later on, this measuring was automated as described in Chapter 2.5.2. Data obtained by this pattern were later processed in Python.

To verify the correctness of data processing from the previous type of measurement a constant voltage setup was used. After the measurement was turned on, the tip was held at a constant level until resistance was more or less stabilized, then it was raised and all over again as long as the tip remained submerged in the droplet.

For most measurements, at first voltage was changed as described previously, then the distance between the top-gate electrode and the sample would be changed and new measuring turned on.

2.2.2. Results and discussion

For each set of measurements, the transport response was measured at 14 different distances, with $d \in \langle 0, 1680 \rangle$ µm. Some of the results can be seen in Fig. 2.2. There are clearly visible two maxima, both are Dirac points, which are formed due to the hysteretic behaviour of graphene. The one on the right is formed during the first voltage increase from 0 V to 1.5 V and the second one during voltage decrease from 1.5 V to -1.5 V.

Such a procedure was repeated with deionized water and three concentrations of dopamine solution. They were later put in one graph for each distance to compare how

the Dirac point changes depending on concentration and distance. For a better overview, only the first quarter of each set of measurements was used in Fig. 2.3. This way the first (right) Dirac point for every concentration and distance can be clearly seen; the second (left) Dirac point does not change enough to show plainly visible differences in this type of chart.
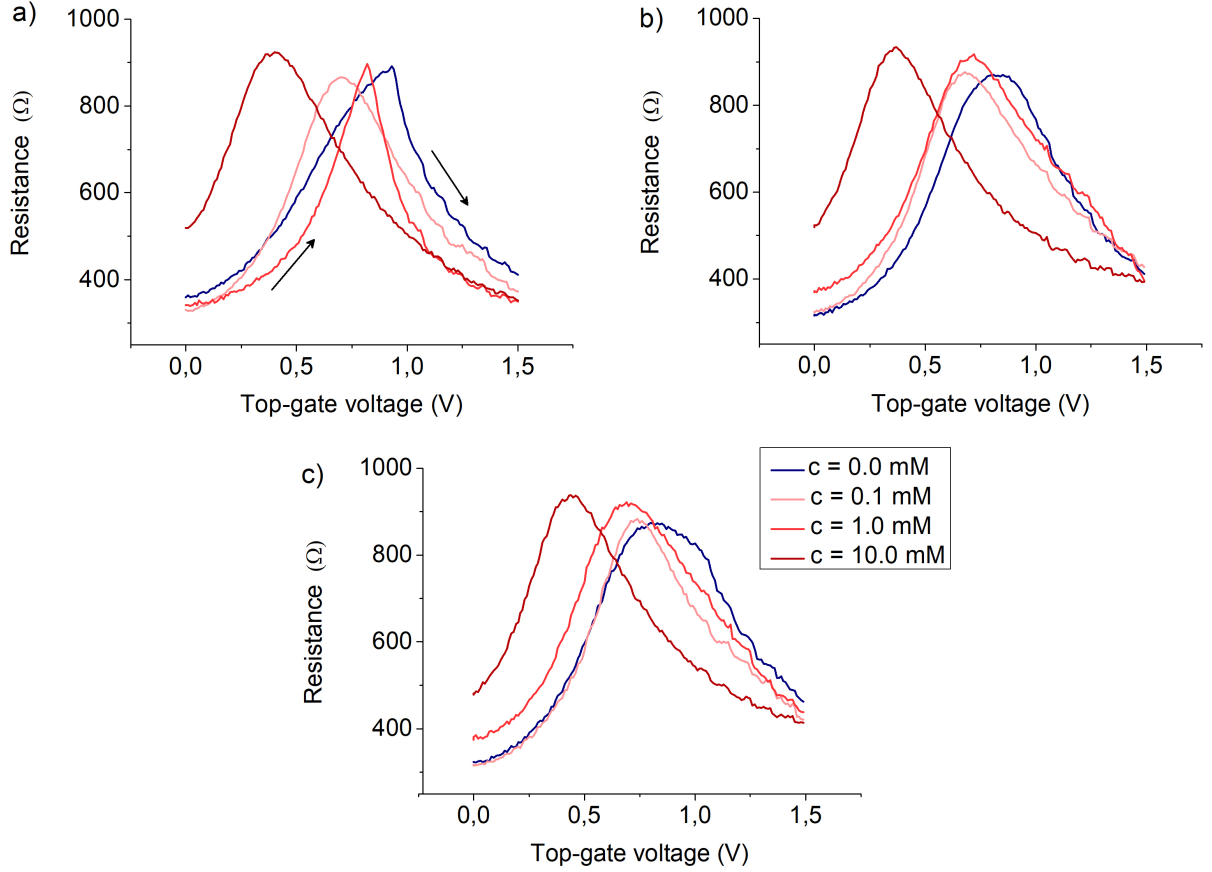
Figure 2.3: Top-gate transport response of different dopamine solution concentrations at distance: a) 10 μm, b) 380 μm and c) 1380 μm; legend valid for all subfigures.

Table 2.1: Dirac point voltage and resistance dependency on concentration (c) and distance (d).

| d (μm) | c = 0.0 mM | | c = 0.1 mM | | c = 1.0 mM | | c = 10 mM | |
	V_{DP} (V)	R (Ω)	V_{DP} (V)	R (Ω)	V_{DP} (V)	R (Ω)	V_{DP} (V)	R (Ω)
10	0.92	891.14	0.7	866.11	0.82	897.1	0.4	923.03
380	0.81	869.98	0.69	876.24	0.73	917.07	0.38	933.46
1380	0.8	874.45	0.75	883.1	0.7	921.54	0.45	937.93

As can be observed in Fig. 2.3 and Tab. 2.1, with increasing concentration, the Dirac point can be found at a lower voltage, therefore it is safe to estimate that dopamine functions as a donor and causes n-doping on graphene FET.

But, how does the shift of the Dirac point voltage of each individual concentration on distance depend? This question is difficult to answer, as even after 30 different sets of measurement the data are inconclusive.

Fig. 2.4 b) shows an example of what most of the charts look like. Data were obtained by finding Dirac points, and then voltage at zero distance of each concentration was subtracted from the voltage at every distance of the same concentration. Thus the shift of voltage was calculated.

Though data differed a lot, more than 50 % of data of dopamine solutions had the tendency to shift to a lower voltage and then stabilize or slightly rise, on the other hand water remained rather constant or rose.
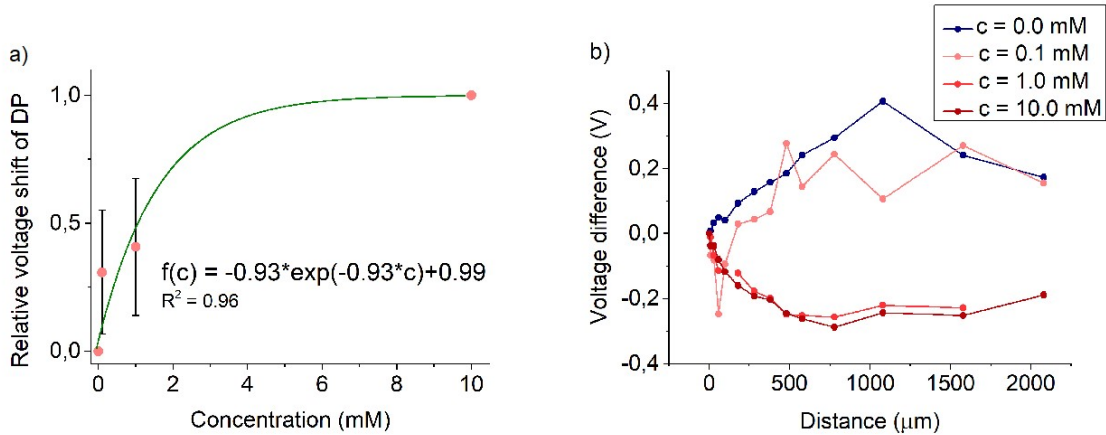

Figure 2.4: a) Relative shift of V_{DP} compared to the shift of dopamine 10 mM from water; b) The change of the first Dirac point voltage compared to the voltage at zero distance for each concentration.

However, Fig. 2.4 a) shows the dependency of the mean V_{DP} calculated from all used measurements regardless of the distance (because there was no clear distance dependency) on concentration. By using the interpolated function, approximate concentration of an unknown dopamine solution could be determined if a water solution and solution with known dopamine concentration were measured at the same time and on the same sample.

Probably the most interesting results are in Fig. 2.5 a), b) which show the dependency of Dirac point resistance on distance. Now how were these graphs obtained?

First of all, the Dirac point voltage and the corresponding resistance were found. Then, because the desire was to see how the resistance at a certain voltage shifts depending on distance, the lowest voltage of Dirac point for the set of measurements was found - it would be inconvenient to analyse resistance at voltage laying in between the V_{DP}'s. To study the resistance of voltages on the left from all Dirac points, voltage in range $\langle 0.05, 0.70 \rangle$ V with the step $\Delta V = 50$ mV was subtracted and a graph was created for resistance at each of these voltages. It would be possible to find the highest V_{DP} and add voltage to study the resistance on the right of all Dirac points, but as the V_{DP} were often located at more than 1 V, then after adding the voltage shift, the voltage would soon be out of range. Therefore it was opted to study resistance at voltages smaller than the lowest V_{DP}.

It cannot be said at exactly which voltage was the resistance taken in general, because that differs for every concentration and even for every measurement of one concentration (as it depends on the sample, graphene purity and dislocations, humidity between

graphene and electrodes,...), but every concentration is plotted at the same voltage shift from the lowest Dirac point voltage. These values were in range from 700 Ω to 1400 Ω. To better see the resistance evolution in the chart, the lowest resistance of each concentration was subtracted.

Unlike with the Dirac point voltage, here the results are conclusive and very well observable in Fig. 2.5. Graphs with the voltage shift of 0.25 V and 0.7 V to the left of all Dirac points were chosen to this thesis because they were the most consistent and provable. With resistance at a certain voltage lower than the Dirac point voltage, all Dopamine solutions tend to linearly rise at close proximity of the top-gate probe to the graphene channel, and then gradually stabilize and become independent on distance increase.

Such a result supports the theory foreshadowed in Chapter 1.2.1., where equation (1.6) suggests two possible outcomes. Either resistance would be constant if the Debye length was not affected by the near presence of the top-gate electrode or resistance would linearly rise with the distance between the gate and the sample influencing a change to Debye length.
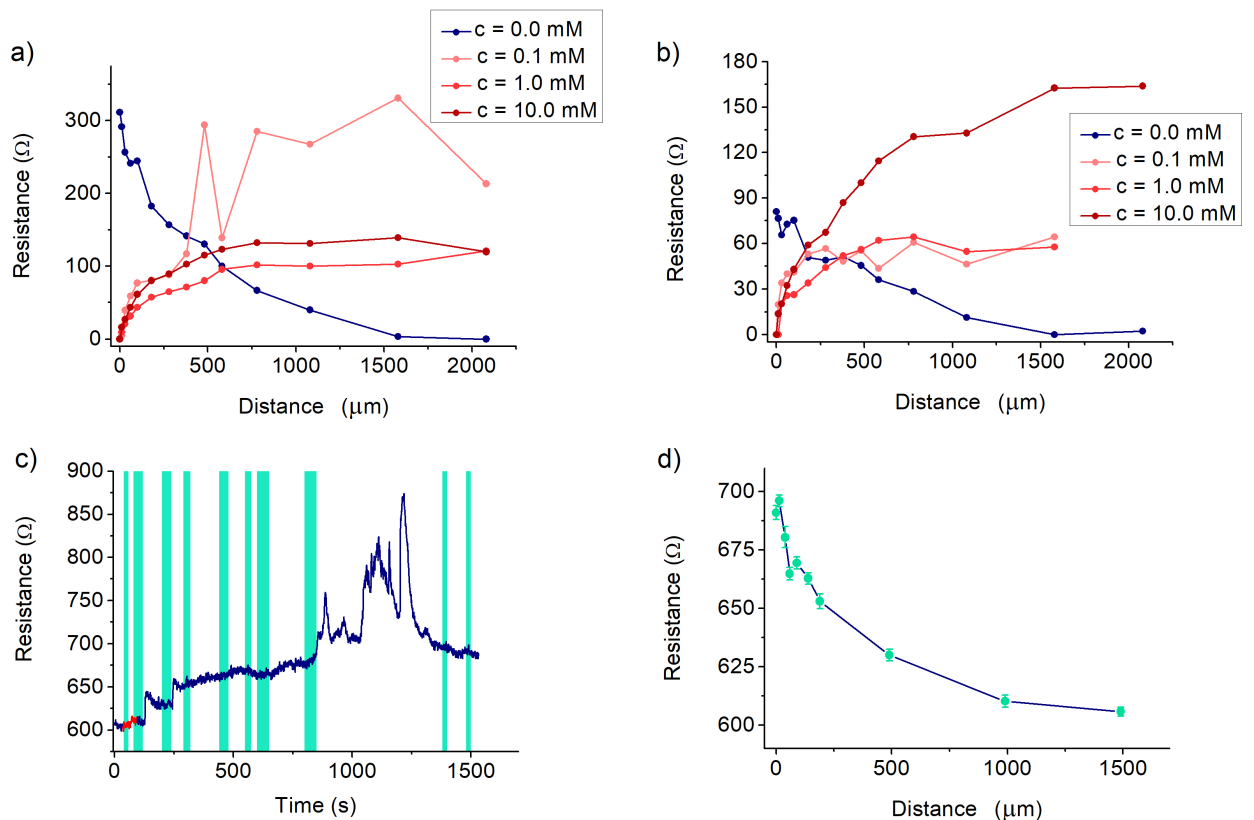
Figure 2.5: Change of the first (right) Dirac point resistance compared to the lowest resistance of each concentration (at a zero distance for dopamine solutions and at the furthest distance for water) at a) -0.25 V and b) -0.70 V from the lowest Dirac point voltage of each concentration; c) the resistance of water measured in time at the constant voltage of 1 V (on the left from the Dirac point) applied on gate while reducing distance after stabilization of resistance; d) the mean resistance from the previous figure at each distance.

In the end, it seems that the resistance of dopamine solution measured at smaller distances is in fact subjected to the change of distance, however at distances much greater than Debye length, the resistance remains invariable.

Nevertheless, the difference of resistance depending on distance of water is quite different from the one of dopamine solutions. At smaller distances, the resistance quickly drops and then is slowly stabilized. This behaviour is in direct variance with the theory in Chapter 1.2.1. and is not fully understood so far, but a control measurement was done and, as is to be seen in Fig. 2.5, agrees with previous data.

2.3. Bottom-gate GFET biosensor

2.3.1. Measurement procedure

The process of bottom-gate measuring is similar to the top-gate procedure. The main difference is that there is no movement of the gate probe; the distance between the gate and graphene channel is constant. Compliance is set to 80 V (as a resistance of SiO_2 is very high). Once again the saw voltage is used starting at 0 V, however increasing up to 50 V, decreasing to -50 V, and coming back to 0 V.

2.3.2. Results and discussion

Bottom-gate transport response was measured with the use of the same sample as most of the data for top-gate response. Similarly to the top-gate transport response, the Dirac point of the bottom-gate transport response shifts significantly to a lower gate voltage with growing concentration, suggesting a negative doping again (Fig. 2.6).

The peak around the V_{DP} for deionized water is not symmetrical. This might occur if the carrier mobility of holes (on the right from V_{DP}) is smaller then the one of electrons.
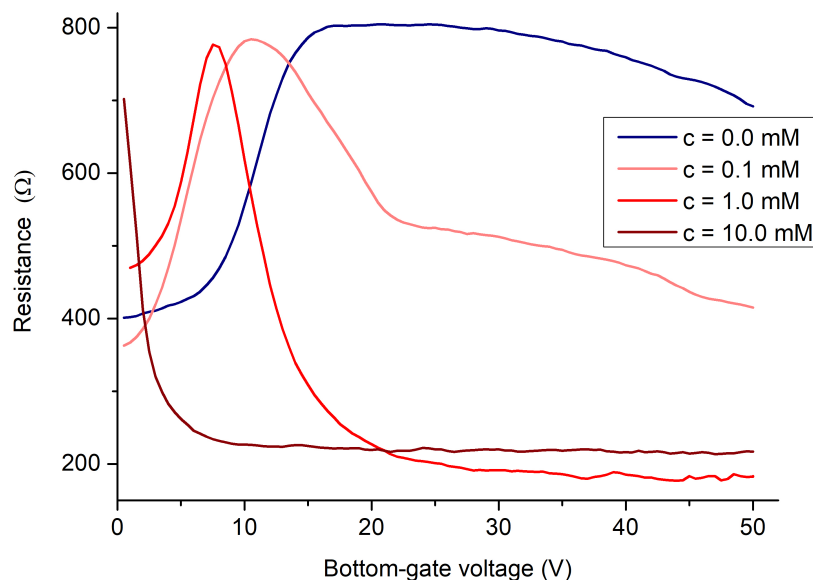

Figure 2.6: Bottom-gate transport response for different Dopamine solution concentration.

Note: Both Dirac points were clearly visible, however upon reaching -15 V, only a high level of noise was measured, which was probably caused by the gate being breached. But, when again reaching -15 V while voltage was being increased, the noise became negligible and reasonable data were measured once again. Because of the demand to do all measurements on one sample, the measuring range was modified to only drop the voltage to -15 V and immediately start raising back to 0 V.

2.4. Dual-gate GFET biosensor

2.4.1. Experimental setup

The experimental setup is very similar to the top-gate setup. The difference is that it is necessary to connect another current source to the bottom gate, which is not controlled by the LabView program but manually.

2.4.2. Measurement procedure

The dual-gate transport response measurement is almost the same as the top-gated one, only instead of changing the distance, a bottom-gate voltage is changed between each measurement.

Therefore, three pins are plugged in (source, drain and bottom gate), compliance for top-gate is set to 2 V, a saw voltage in a range (-1.5, 1.5) V is created and on the other current source compliance for the bottom gate is set to 80 V with desired current (counted from the desired voltage).

Then one top-gate transport response is measured, the bottom gate is switched off, current is changed and again the gate is switched on, another measurement can start. However, due to the apparatus's capacitor-like behavior it is important to wait until the resistance is stabilized.

Table 2.2: Table shows the set voltage of bottom-gate and the final real voltage measured between ground and bottom gate electrodes.

V_{set} (V)	0	2	4	6	8	10	12	14	16	18	20
V_{real} (V)	0	1.8	3.6	5.4	7.1	8.0	9.5	10.2	12.7	13.5	14.3

Due to a remaining charge, resistance of outer electrodes or long cables, the real voltage does not correspond to the set one. Set values and the real values measured by an external multimeter are summarised in Tab. 2.2

2.4.3. Results and discussion

Data acquired from dual-gate transport response (Fig. 2.7 a), b)) show that the bottom-gate voltage causes a significant shift of the first Dirac point to the left towards smaller and even negative top-gate voltage. This effect is more visible with a higher concentration of dopamine solution. However, the tendency of the Dirac point voltage to shift with bottom-gate voltage change is clearly observable with deionized water as well.
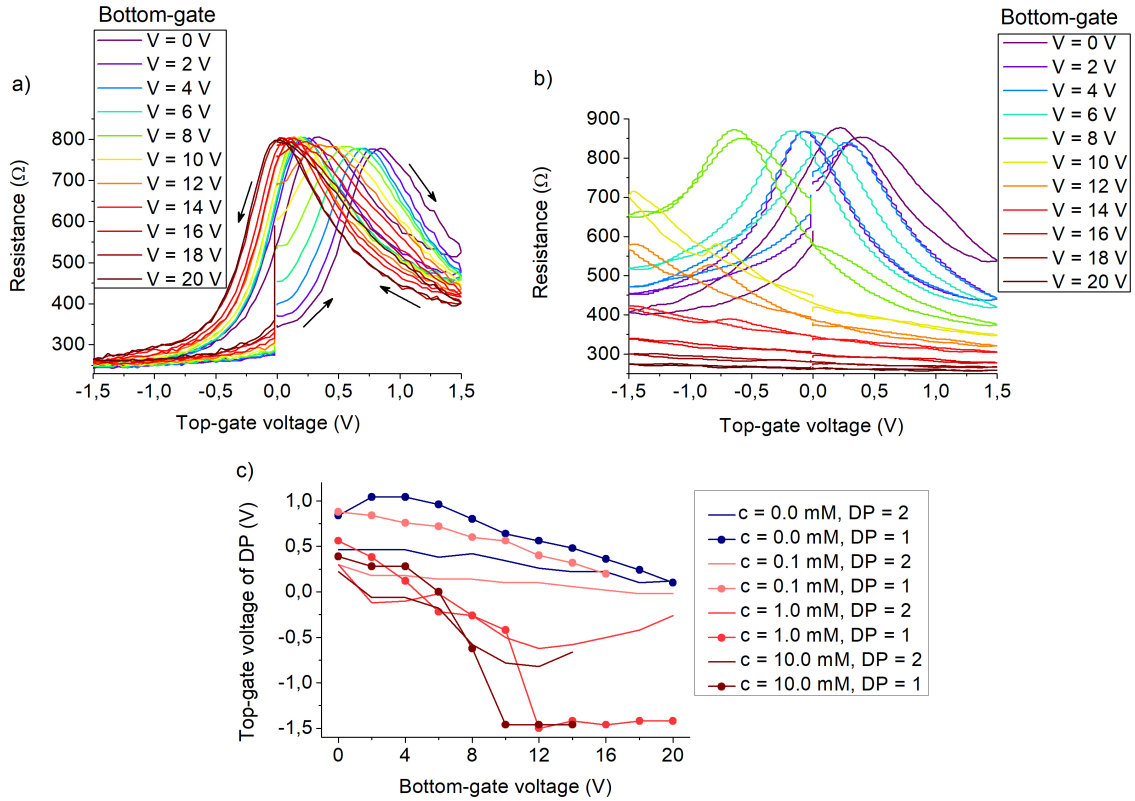
Figure 2.7: Resistance as a function of top-gate voltage at constant values of bottom gate voltage for dopamine concentrations of a) 0.1 mM and b) 10.0 mM solution; c) both Dirac points voltage dependency on bottom gate for different solution concentrations.

Furthermore the second Dirac point does not shift very much compared to the first Dirac point, the shift is almost negligible with water and dopamine 0.1 mM concentration. The change in Dirac point voltage is shown in Fig. 2.7c).

Another interesting outcome is that with higher bottom-gate voltage rises the level of noise and resistance goes down. This effect is more relevant especially with more concentrated solutions, which makes it very difficult to even find Dirac points for dopamine 10 mM at a higher bottom-gate voltage than 14 V.

The reason for the second Dirac point not moving may be because of hysteresis. The sample had once already been through applied voltage, had the time to accommodate to the change and rearrange free charge carriers.

The shift of the first Dirac point towards lower voltage might be useful when trying to measure top-gate transport response. As the nature of GFET is to be p-doped due to impurities and defects which sometimes cause the Dirac point to be out of the measurable range (especially when p-doping solution is added), applying small bottom-gate voltage could help to see at least the first Dirac point.

2.5. Improvements in measurement

2.5.1. Anti-evaporation chamber

One of the biggest problems that had to be addressed was the quick evaporation of the solution. Given one top-gate measuring took about 1.5 hours, even a solution droplet of 50 μl evaporated to approximately half its former radius, hence the volume was eight times smaller. The dopamine in the solutions did not evaporate, so the concentration at the end of one set of measurements increased eight times.

The solution to this issue was to approach relative humidity to 100 % (saturation) to limit evaporation or even stop it. A humidity chamber was thought of, but the one available would make it impossible to move the top gate electrode which was crucial, therefore a new device had to be made.
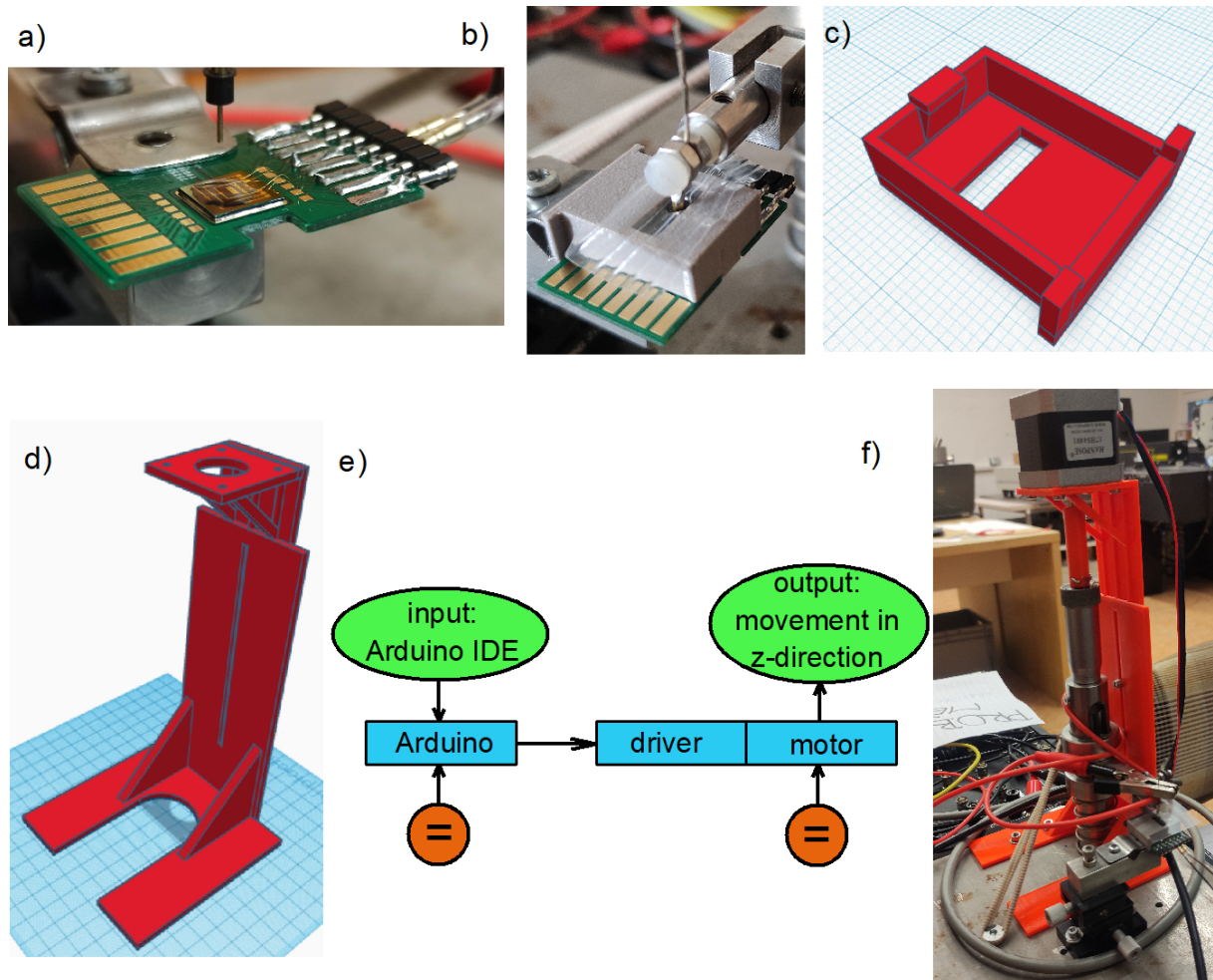

Figure 2.8: a) Photo of the sample and the distanced top-gate tip after the end of top-gate measuring; b) the sample with an anti-evaporation chamber; c) bottom-up anti-evaporation chamber prepared for printing; d) motor holder prepared for printing; e) a scheme of the automation system for z-direction movement; f) a construction for automation.

The anti-evaporation chamber in Fig. 2.8 c) was designed in Tinkercad to fit the holder that was used, then printed on a 3D printer. On one side it has a protrusion that fits perfectly in a cutout of the base used for preventing any movement when it is stored in a box, on the opposite side there are two more protrusions. Those come above and from the sides of the metal base holder. Together they avert the anti-evaporation chamber from any movement, which could lead to golden contacts breaking or the sample scratching.

At the top of the box is a window for the insertion of the top-gate electrode, which had to be big enough to enable measuring right above any one of the three pairs of electrodes on the sample. There are three pairs of source and drain electrodes (two pairs working as back-up system) to allow for more measurements using one graphene sample. To prevent vapour leakage, this window was always covered by a foil with a hole for the top-gate electrode. This foil could slide on the top of the box.

At the side of the chamber where the two protrusions are, a foam was glued to its face. The foam was soaked up with deionised water to elevate the humidity.

With the anti-evaporation chamber being used, it was not possible to tell by the naked eye any difference in the size of the droplet before and after measurement.

2.5.2. Automation of top-gate measurement

As was described in Chapter 2.2.1., for most of the top-gate measurements it was required to spin a micrometer screw to slightly change the distance between the top-gate electrode and the sample surface. This procedure had to be done every six minutes for each new top-gate trace measuring with different parameters. As a set of 14 measurements was done, one person was required to be present for an hour and a half and to pay close attention to the time to change the z-direction. As a result, the possibility of using automation was considered.

For automation, a step motor Nema 17 was fixed on top of a holder (Fig. 2.8 f)) designed in Tinkercad and printed on a 3D printer. A narrow conjunction was printed to connect the motor shaft with the top part of the micrometer screw used for its spinning.

For the step motor to work as desired, C++ language program Arduino IDE was used. The written program was uploaded to an Arduino microcontroller and together with a driver controlled the motors' rotation. Arduino was powered by a USB directly from the computer used for measuring and the step motor was powered by 22 V from a laboratory power supply.

Conclusion

The aim of the thesis was to investigate the interaction between dopamine solution and graphene using a field-effect transistor and so creating a dopamine biosensor. The goals were to study the transport response of the biosensor to different concentrations of dopamine solution in the dependency on gate voltage and on the distance between the top-gate electrode submerged into the solution and graphene. Furthermore, various combinations of top and bottom gate settings were tested and the last goal was to suggest more efficient techniques of measuring. All the goals were fulfilled.

The most comprehensive measurements were done with the top-gate electrode and multiple factors were studied. First and most importantly, the Dirac point voltage shifted to lower gate voltage with increasing concentrations of dopamine in every realised measurement, hence it can be said that n-doping was observed and that dopamine acts as donor.

The dependency of the V_{DP} on distance was not proven, each set of measurements differed a lot in these characteristics.

From the assumption that the dependency of the V_{DP} on the distance is random, all measurements regardless of the distance and the gate used were put together to show a graph depending on the concentration of dopamine. Knowing that there is an exponential dependency, this could be used for determining the concentration of an unknown dopamine solution.

The last tracked dependency was that of the resistance at a selected voltage on distance. It was confirmed that at close distance (up to 100 µm) the resistance has the tendency to quickly rise and then slowly stabilize. This corresponds to the theory. On the other hand, it is quite interesting that the behaviour of water is very different, the resistance tends to drop and then stabilize; this is not fully understood yet.

The bottom-gate measurements confirmed what was known from the top-gate measurements - increasing concentrations of dopamine solutions shift the Dirac point voltage towards lower gate voltage, corresponding to n-doping of graphene.

Measurements accomplished with the use of both gate electrodes promise easier measuring in the future. The addition of the bottom-gate voltage, which was held constant over one transport response measurement, modulated the response significantly. The increase of the bottom-gate voltage led to an increase of measured noise and to a decrease of the range of resistance (from $\Delta R = 500 \ \Omega$ to $\Delta R = 30 \ \Omega$). On the other hand, the V_{DP} shifted considerably towards lower top-gate voltage and at higher concentration even to negative voltage. This could be used in top-gate measurements, if the sample is too p-doped that the V_{DP} is outside of the possible voltage range.

In the end two improvements were made to the measurements. The first of them was the construction of an anti-evaporation chamber and the second was the automation of the top-gate electrode movement in the z direction.

Bibliography

[1] SCHEDIN, F., GEIM, A. K., MOROZOV, S. V., HILL, E. W., BLAKE, P., KAT-SNELSON, M. I., NOVOSELOV, K. S. (2007). Detection of individual gas molecules adsorbed on graphene. Nature Materials, 6(9), 652-655.

[2] LI, Y., ZHANG, Y., XU, J., TAO, C. (2010). Biological applications of graphene and graphene oxide. Frontiers of Physics, 5(3), 252-258.

[3] PUMERA, M., AMBROSI, A., BONANNI, A., CHANG, E. L. K., POH, H. L. (2010). Graphene for electrochemical sensing and biosensing. TrAC Trends in Analytical Chemistry, 29(9), 954-965.

[4] LU, C. H., YANG, H. H., ZHU, C. L., CHEN, X., CHEN, G. N., ZHANG, X. J. (2019). A graphene platform for sensing biomolecules. Angewandte Chemie International Edition, 51(25), 1770-1774.

[5] MUELLER, T., XIA, F., AVOURIS, P. (2015). Graphene photodetectors for high-speed optical communications. Nature Photonics, 4(5), 297-301

[6] JUÁREZ OLGUÍN, H., CALDERÓN GUZMÁN, D., HERNÁNDEZ GARCÍA, E., BARRAGÁN MEJÍA, G. The Role of Dopamine and Its Dysfunction as a Consequence of Oxidative Stress. Oxid Med Cell Longev. 2016;2016:9730467. doi: 10.1155/2016/9730467. Epub 2015 Dec 6. PMID: 26770661; PMCID: PMC4684895.

[7] Wikipedia contributors. Ventral tegmental area [online]. In: Wikipedia, The Free Encyclopedia. [Accessed 11 May 2023]. Available from: https://en.wikipedia.org/wiki/Ventraltegmentalarea.

[8] Hazelden Betty Ford Foundation. Drug Abuse and the Brain [online]. [Accessed 11 May 2023]. Available from: https://www.hazeldenbettyford.org/research-studies/addiction-research/drug-abuse-brain.

[9] Cleveland Clinic. Dopamine Deficiency [online]. [Accessed 11 May 2023]. Available from: https://my.clevelandclinic.org/health/articles/22588-dopamine-deficiency.

[10] PAPAGEORGIOU, D., KINLOCH, I., YOUNG, R. (2017). Mechanical Properties of Graphene and Graphene-based Nanocomposites. Progress in Materials Science. 90. 10.1016/j.pmatsci.2017.07.004.

[11] BONACCORSO, F. et al. Graphene photonics and optoelectronics. Nat Photonics. 2010;4(9):611-622

[12] BÉRAUD, A., SAUVAGE, M., BAZÁN, C.M., TIE, M., BENCHERIF, A., BOUILLY, D. Graphene Field-Effect Transistors as Bioanalytical Sensors: Design, Operation, and Performance. Analyst. 2021;146(2):403-428. doi: 10.1039/d0an01661f. Epub 2020 Nov 20. PMID: 33215184.

[13] NOVOSELOV, K.S. et al. Electric Field Effect in Atomically Thin Carbon Films. Science. 2004;306(5696):666-669. doi: 10.1126/science.1102896. ISSN: 0036-8075.

[14] HERZÁNOVÁ, K.Detekce fragmentů DNA/RNA pomocí grafenového senzoru a vliv horního elektrolytického hradla. Brno: Brno University of Technology, Faculty of Mechanical Engineering, 2022. 42 p. Supervisor doc. Ing. Miroslav Bartošík, Ph.D

[15] MIKHAILOV, S. Frequency Mixing Effects in Graphene. 10.5772/13832.

[16] BIRO, L., NEMES-INCZE, P., LAMBIN, P. (2011). Graphene: Nanoscale processing and recent applications. Nanoscale, 4, 1824-1839. doi:10.1039/c1nr11067e.

[17] SUPALOVÁ, Linda. Detection of biochemical substance using graphene sensor. Brno, 2021, 52 p. Bachelor's Thesis. Brno University of Technology, Faculty of Mechanical Engineering, Institute of Physical Engineering. Advised by doc. Ing. Miroslav Bartošík, Ph.D.

[18] LEE, C., WEI, X., KYSAR, J. W., HONE, J. Measurement of the elastic properties and intrinsic strength of monolayer graphene. Science, 321(5887), 385-388. doi: 10.1126/science.1157996. PMID: 18635798.

[19] NAIR, R. R., BLAKE, P., GRIGORENKO, A. N., NOVOSELOV, K. S., BOOTH, T. J., STAUBER, T., PERES, N. M. R., GEIM, A. K. Fine Structure Constant Defines Visual Transparency of Graphene. Science, 320(5881), 1308-1308. ISSN 0036-8075. doi: 10.1126/science.1156965

[20] BALANDIN, A. A., GHOSH, S., BAO, W., CALIZO, I., TEWELDEBRHAN, D., MIAO, F., LAU, C. N. Superior Thermal Conductivity of Single-Layer Graphene. Nano Letters, 8(3), 902-907. ISSN 1530-6984. doi: 10.1021/nl0731872.

[21] NOVOSELOV, K., FAL'KO, V., COLOMBO, L., et al. A roadmap for graphene. Nature, 490, 192-200 (2012).

[22] XU, Y., CAO, H., XUE, Y., LI, B., CAI, W. (2018). Liquid-Phase Exfoliation of Graphene: An Overview on Exfoliation Media, Techniques, and Challenges. Nanomaterials (Basel), 8(11), 942. doi:10.3390/nano8110942. PMID: 30445778; PMCID: PMC6265730.

[23] MARTINEZ, A., FUSE, K., YAMASHITA, S. (2011). Mechanical exfoliation of graphene for the passive mode-locking of fiber lasers. Applied Physics Letters, 99(12), 121107.

[24] CHEN, J., ZHANG, Y., LI, W., LIU, L., LI, H., LIANG, J. Chemical vapor deposition growth of graphene: Toward large-scale production and control. Advanced Science, 3(10), 1500261.

[25] HUANG, J., MA, L., CHEN, Y., ZHANG, Y., LI, W., DAI, L. Recent advances in controlled nucleation and growth of large-area homogeneous graphene films. Chemistry of Materials, 30(6), 1805-1816

[26] KIM, J., PARK, S., HONG, B. H. Role of metal substrates in the growth of large-area monolayer graphene. Accounts of Chemical Research, 48(1), 60-68

[27] YANG, W., GONG, Y., ZHANG, J. Controlled growth of large-area and high-quality single-layer graphene film by chemical vapor deposition. Frontiers in Chemistry, 7, 756

[28] TRIKKALIOTIS, D.G., CHRISTOFORIDIS, A.K., MITROPOULOS, A.C., KYZAS, G.Z. (2021). Graphene Oxide Synthesis, Properties and Characterization Techniques: A Comprehensive Review. ChemEngineering, 5, 64. doi: 10.3390/chemengineering5030064.

[29] COOPER, D. R., D'ANJOU, B., GHATTAMANENI, N., HARACK, B., HILKE, M., HORTH, A., MAJLIS, N., MASSICOTTE, M., VANDSBURGER, L., WHITEWAY, E. ISRN Condens. Matter Phys., 2012, 501686 (2012).

[30] GEIM, A. K., NOVOSELOV, K. S. The rise of graphene. Nature Materials, 6(3), 183-191

[31] HWANG, M.T., HEIRANIAN, M., KIM, Y. et al. Ultrasensitive detection of nucleic acids using deformed graphene channel field effect biosensors. Nat Commun, [S.l.], v. 11, p. 1543, 2020. DOI: 10.1038/s41467-020-15330-9.

[32] VOLKOW, N.D.; WISE, R.A. How can drug addiction help us understand obesity? Nat Neurosci, [S.l.], v. 8, n. 5, p. 555-560, 2005. DOI: 10.1038/nn1452. PMID: 15856062.

[33] MEISER, J., WEINDL, D., & HILLER, K. (2013). Complexity of dopamine metabolism. Cell Communication and Signaling, 11(1), 34.

[34] BEAULIEU, J.M., GAINETDINOV, R.R. (2011). The Physiology, Signaling, and Pharmacology of Dopamine Receptors. Pharmacological Reviews, 63(1), 182-217. Retrieved from doi:10.1124/pr.110.002642.

[35] SCHULTZ, W. Dopamine reward prediction error coding. Dialogues in Clinical Neuroscience, [S.l.], v. 18, n. 1, p. 23-32, 2016.

[36] LAMMEL, S.; LIM, B. K.; MALENKA, R. C. Reward and aversion in a heterogeneous midbrain dopamine system. Neuropharmacology, [S.l.], v. 76, Pt B, p. 351-359, 2014.

[37] KAUER, J. A.; MALENKA, R. C. Synaptic plasticity and addiction. Nature Reviews Neuroscience, [S.l.], v. 8, n. 11, p. 844-858, 2007.

[38] LOHR, K. M.; MASOUD, S. T.; SALAHPOUR, A.; MILLER, G. W. Membrane transporters as mediators of synaptic dopamine dynamics: implications for disease. European Journal of Neuroscience, [S.l.], v. 45, n. 1, p. 20-33, Jan. 2017. DOI: 10.1111/ejn.13357. PMID: 27520881; PMCID: PMC5209277.

[39] VOLKOW, N. D.; MORALES, M. The brain on drugs: from reward to addiction. Cell, [S.l.], v. 162, n. 4, p. 712-725, 2015

[40] KALIA, L. V.; LANG, A. E. Parkinson's disease. The Lancet, [S.l.], v. 386, n. 9996, p. 896-912, 2015.

[41] POEWE, W.; SEPPI, K.; TANNER, C. M.; HALLIDAY, G. M.; BRUNDIN, P.; VOLKMANN, J.; ... LANG, A. E. Parkinson disease. Nature Reviews Disease Primers, [S.l.], v. 3, n. 1, p. 1-21, 2017.

[42] HOWES, O. D.; MURRAY, R. M. Schizophrenia: an integrated sociodevelopmental-cognitive model. The Lancet, [S.l.], v. 383, n. 9929, p. 1677-1687, 2014.

[43] KAPUR, S.; MAMO, D. Half a century of antipsychotics and still a central role for dopamine D2 receptors. Progress in Neuro-Psychopharmacology and Biological Psychiatry, [S.l.], v. 27, n. 7, p. 1081-1090, Oct. 2003. DOI: 10.1016/j.pnpbp.2003.09.004. PMID: 14642968.

[44] URBIŠ, J.Optimalizace a měření transportních experimentů na grafenových polem řízených tranzistorech. Brno: Brno University of Technology, Faculty of Mechanical Engineering, 2019. 67 p. Supervisor Ing. Miroslav Bartošík, Ph.D.

[45] PIASTEK, J. Příprava grafenových vrstev pokrytých Ga atomy a charakterizace jejich elektrických vlastností, Brno: Brno University of Technology, Faculty of Mechanical Engineering, 2015. 43 p. Supervisor Ing. Jindřich Mach, Ph.D.

List of abbreviations and symbols used

A	surface area
CVD	chemical vapor deposition
d	distance
D	drain electrode
e	elementary charge
E_F	Fermi energy
FET	graphene field-effect transistor
GFET	graphene field effect transistor
I	ionic strength
I_{sd}	current between the source and the drain
k_B	Boltzmann constant
N_A	Avogadro constant
R	resistance
S	source electrode
Si	silicon
SiO_2	silicon dioxide
T	Temperature
v_d	drift velocity
V_{DP}	Dirac point voltage
V_g	gate voltage
V_{real}	real measured voltage
V_{sd}	voltage between the source and the drain
V_{set}	set voltage
ε_0	permittivity of vacuum
ε_r	relative permittivity
λ_D	Debye length